PHYSICS

Unifying fluctuation-dissipation temperatures of slow-evolving nonequilibrium systems from the perspective of inherent structures

Jianhua Zhang†, Wen Zheng†, Shiyun Zhang, Ding Xu, Yunhuan Nie, Zhehua Jiang, Ning Xu*

For nonequilibrium systems, how to define temperature is one of the key and difficult issues to solve. Although effective temperatures have been proposed and studied to this end, it still remains elusive what they actually are. Here, we focus on the fluctuation-dissipation temperatures and report that such effective temperatures of slow-evolving systems represent characteristic temperatures of their equilibrium counterparts. By calculating the fluctuation-dissipation relation of inherent structures, we obtain a temperature-like quantity T_{IS}. For monocomponent crystal-formers, T_{IS} agrees well with the crystallization temperature T_c, while it matches with the onset temperature T_{on} for glass-formers. It also agrees with effective temperatures of typical nonequilibrium systems, such as aging glasses, quasi-static shear flows, and quasi-static self-propelled flows. From the unique perspective of inherent structures, our study reveals the nature of effective temperatures and the underlying connections between nonequilibrium and equilibrium systems and confirms the equivalence between T_{on} and T_c.

INTRODUCTION

To understand the physics of nonequilibrium systems is one of the major challenges in condensed matter and materials physics (*1*, *2*). An important and core issue of nonequilibrium systems is how to define temperature. In equilibrium systems, there are multiple ways to define temperature, e.g., from thermodynamic fundamental laws, Gibbs relation, transport quantities, fluctuation-dissipation relations (FDRs), kinetic energy, and potential energy, and they all lead to an identical temperature. In nonequilibrium systems, however, although we can still use these definitions, they normally result in different "temperatures," which are called effective temperatures (*3*–*5*). Even in simple systems such as ideal gases and electromagnetic radiation, the definition of nonequilibrium temperature is also a problem (*5*–*7*). Because there are multiple definitions of effective temperatures, each of which has its own meaning, it remains elusive what these effective temperatures really represent.

In this work, we focus on one of the definitions of effective temperatures, the fluctuation-dissipation temperature derived from the FDR. This effective temperature has been paid much attention to and widely adopted in the study of typical nonequilibrium systems such as aging glasses, sheared particulate systems, and active matter. In these systems, the FDR is violated (*8*–*11*). The ratio of the correlation to the response, which is the well-defined heat bath temperature T in thermal equilibrium, has been shown to be time dependent (*11*–*17*). At short times, it is equal to T. At long times, however, it is higher, which has been defined as the effective (fluctuation-dissipation) temperature T_{eff}. The emergence of T_{eff} is expected to have theoretical merit to explain why solid-like states with the heat bath temperature being too low to overcome energy barriers can still undergo structural relaxation under nonequilibrium conditions. Although expected to play an important role in the understanding of nonequilibrium systems,

like other definitions of effective temperatures, it still remains elusive what T_{eff} actually is and whether it is indeed a unique temperature of nonequilibrium systems with abstract physical meanings. People have also put effort into the modification of the FDR under certain nonequilibrium conditions (*7*, *18*, *19*), from which other different effective temperatures could probably be obtained, but these attempts still could not settle the questions above.

In view of the potential energy landscape, the aging of glasses and flowing of particles under shear or self-propulsion are processes that the system moves among different inherent structures (*20*, *21*), i.e., zero-temperature metastable states at local potential energy minima, separated by energy barriers. It has been shown that inherent structures can provide special insight into physics of nonequilibrium systems. For instance, inherent structures have the predictive power of heterogeneous dynamics of supercooled liquids (*22*–*25*), instability and particle rearrangements under excitations (*26*–*29*), and glass transition (*30*). Compared to the success in linking local structural and vibrational properties of inherent structures to specific features of excited nonequilibrium systems, less attention has been paid to the statistical mechanical aspects of inherent structures. Just for the FDR (*9*, *12*–*15*), there has been no attempt yet to investigate whether there is a meaningful relation between some kind of correlation and response of inherent structures. If such a relation could be constructed, a temperature might be derived from it. Such a temperature may shed light on our understanding of effective temperatures from the perspective of zero-temperature solids and thus broaden the predictive power of inherent structures.

Here, we implement the calculation of the density correlation and response of inherent structures. A quantity with the temperature dimension, T_{IS}, is derived from their ratio. For several widely studied model systems in both two (2D) and three (3D) dimensions, T_{IS} agrees well with the crystallization temperature of monocomponent systems and the onset temperature (to be defined later) of glassformers. We also compare T_{IS} of inherent structures obtained from the fast quenching of high-temperature states with that of ultrastable inherent structures obtained from the swap Monte Carlo algorithm (*31*), corresponding to extremely slow quenching, and find

Hefei National Laboratory for Physical Sciences at the Microscale, CAS Key Laboratory of Microscale Magnetic Resonance, Department of Physics, University of Science and Technology of China, Hefei 230026, P. R. China.
*Corresponding author. Email: ningxu@ustc.edu.cn
†These authors contributed equally to this work.

identical results. Note that we deal with nonequilibrium systems in the absence of dynamics (i.e., at zero temperature), so it is not straightforward that the calculation could lead to equilibrium temperatures. This finding builds up the links between nonequilibrium and equilibrium systems and between onset and crystallization temperatures and suggests an indirect way to obtain characteristic temperatures of equilibrium systems. Driven by the curiosity about whether the agreement between T_{IS} and equilibrium temperatures hints anything about effective temperatures in slow-evolving nonequilibrium systems, we directly calculate effective temperatures for aging glasses and quasi-static flows of sheared and self-propelled systems and find that they all agree well with T_{IS}.

RESULTS
FDR of inherent structures

To show that our results are not just for a chosen system, here, we study three types of widely used model systems over a wide range of densities, with harmonic (HARM), Lennard-Jones (LJ), and repulsive LJ (RLJ) particle interactions, respectively (see Materials and Methods for the details). We also study mono-, bi-, and polydisperse systems for diversity. We choose the Fourier transform of the density

$$\rho_k = \frac{1}{N'}\sum_j \xi_j \exp\left(i\vec{k}\cdot\vec{r}_j\right) \tag{1}$$

as the observable, where N' is the number of large particles for bidisperse systems and is equal to the total number of particles N for mono- and polydisperse ones, the sum is over all N' particles, $\vec{k} = k\hat{x}$ is the wave vector along the x direction satisfying the periodic boundary conditions, $\vec{r}_j$ is the location of particle j, and ξ_j is randomly chosen to be 1 or -1 with a zero mean. As most of previous studies, we choose k to be approximately the value at which the static structure factor reaches the first maximum, which quantifies the average separation between nearest neighbors. We apply a weak external field by introducing a perturbation (9, 32)

$$\Delta H = -h\rho_k \tag{2}$$

to the Hamiltonian, where h is the strength of the field. This leads to an external force $-\nabla_j(\Delta H)$ on particle j. In most of our studies, inherent structures are obtained by quenching high-temperature states to local energy minima at a given density and in the presence of a given external field via the fast inertial relaxation engine (FIRE) minimization algorithm (33). Then, we decrease h by a small step size δh and perform the FIRE minimization again. We repeat this procedure until h decays to zero. In the small h limit, we obtain the linear response

$$R = \lim_{h\to 0}\frac{\langle\rho_{k,IS}\rangle_h - \langle\rho_{k,IS}\rangle_0}{h} \tag{3}$$

where $\rho_{k,IS}$ denotes the density of inherent structures, and $\langle.\rangle$ denotes the ensemble average with the subscript showing the field. For inherent structures with $h = 0$, we also calculate the correlation

$$C = \langle\rho_{k,IS}^2\rangle_0 - \langle\rho_{k,IS}\rangle_0^2 \tag{4}$$

where $\langle.\rangle$ also denotes the ensemble average. Borrowing the FDR, we define a temperature-like quantity

$$T_{IS} = \frac{C}{R} \tag{5}$$

The expression of T_{IS} has exactly the same form of the effective temperatures derived from the FDR in previous studies (10–17), only that, here, T_{IS} is calculated directly from zero-temperature states in the absence of dynamics. It is not straightforward to tell whether T_{IS} can be a meaningful temperature and whether it can be related to effective temperatures of evolving systems with dynamics.

To check whether T_{IS} relies on quench rate, we also calculate T_{IS} of ultrastable inherent structures. To obtain an ultrastable state, we first equilibrate a polydisperse system at a temperature lower than the glass transition temperature using the swap Monte Carlo algorithm (31) and then quench the system to the local minimum via FIRE. The resultant ultrastable inherent structures can be viewed as states quenched with extremely slow rates. In the following, if not specified, the results are for fast-quenched inherent structures.

We first focus on mono- and bidisperse systems in 3D. Figure 1 shows the density evolution of R, C, and T_{IS}. For both LJ and RLJ systems, Fig. 1A shows that the response R monotonically decreases when the density ρ increases. Over the range of densities studied, R changes over a decade. In contrast, the correlation C varies more mildly, fluctuating by at most a factor of two, as shown in Fig. 1B. Therefore, the density dependence of T_{IS} is mainly determined by $R(\rho)$. As shown in Fig. 1C, T_{IS} monotonically increases with ρ for both mono- and bidisperse systems. At high densities, RLJ and LJ systems behave quantitatively the same, where attraction in LJ systems acts just as a small perturbation (30, 34–36). With the decrease
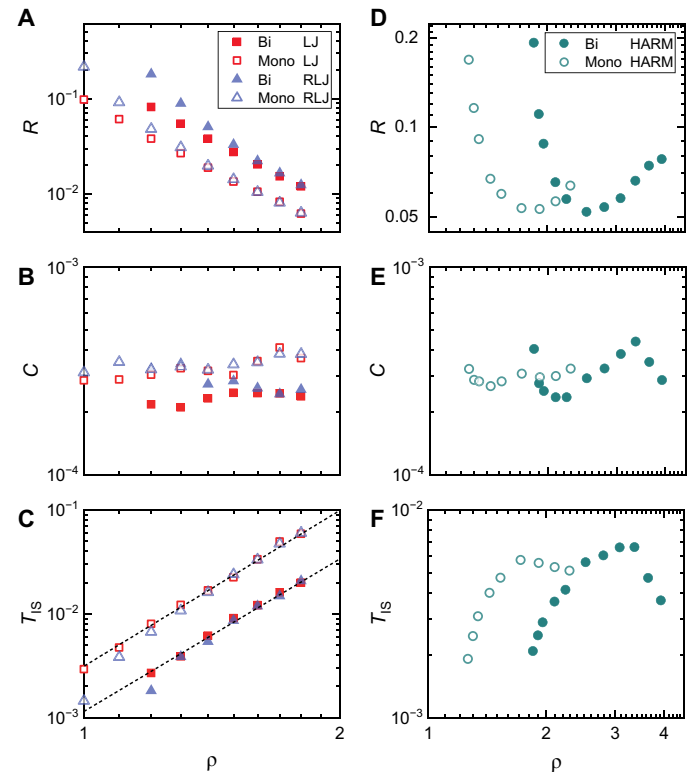
Fig. 1. Temperature-like quantity from inherent structures in 3D. (**A** to **C**) Density ρ dependence of the response R, the correlation C, and the temperature-like quantity T_{IS} for LJ and RLJ systems, respectively. Dashed lines in (C) shows the $T_{IS} \sim \rho^5$ scaling. (**D** to **F**) are for HARM systems.

of ρ, they depart from each other and the bifurcation is more and more pronounced, indicating the growth of the nonperturbative role of attraction (*30, 35, 36*). The presence of attraction helps to stabilize LJ systems at low densities, leading to a smaller response and consequently a higher T_{IS}.

Figure 1D indicates that the $R(ρ)$ of HARM systems is qualitatively different from those of RLJ and LJ systems. With the increase of ρ, R initially decreases but increases after reaching a minimum. Because $C(ρ)$ also varies relatively mildly (see Fig. 1E), this nonmonotonic behavior of $R(ρ)$ results in a nonmonotonic $T_{IS}(ρ)$. As shown in Fig. 1F, $T_{IS}(ρ)$ exhibits a maximum.

Agreement between T_{IS} and characteristic temperatures of equilibrium systems

The density dependence of T_{IS} resembles some well-known liquid-solid transition temperatures, e.g., the crystallization temperature and the glass transition temperature. RLJ and LJ potentials have the same repulsive core, only that the LJ potential has an attractive tail. It has been shown that the glass transition temperature of LJ systems is higher than that of RLJ systems at low densities due to the nonperturbative role of attraction (*30, 35, 36*). At high densities, the glass transition temperatures of LJ and RLJ systems are almost identical and show a power-law scaling with density: $T_g^{LJ} \approx T_g^{RLJ} \sim ρ^γ$ with $γ \approx 5$ (*30, 36–38*). All these features are reproduced in $T_{IS}(ρ)$. As shown in Fig. 1C, $T_{IS}^{LJ} \approx T_{IS}^{RLJ} \sim ρ^5$ at high densities and $T_{IS}^{LJ} > T_{IS}^{RLJ}$ at low densities. Note that the crystallization temperature should have similar density dependence to the glass transition temperature (*30, 35, 36, 39–41*). The HARM potential is intrinsically different from LJ and RLJ potentials due to its soft-core nature (*41*). Because of this, HARM systems exhibit reentrant crystallization and glass transition, i.e., the crystallization and glass transition temperatures are nonmonotonic in density and have a maximum value (*25, 41–43*). This reentrant behavior is exactly reproduced in $T_{IS}^{HARM}(ρ)$, as shown in Fig. 1F.

Monodisperse systems are easy to crystallize, so compared to crystallization temperatures, it is not straightforward to determine their glass transition temperatures. In contrast, the bidisperse systems studied here have been widely used as typical glass-formers, which hinder the crystallization. However, for both mono- and bidisperse systems, we obtain $T_{IS}(ρ)$. In addition, note that FIRE minimization always leads to inherent structures with glassy (disordered) structures in 3D (*44*). It is then plausible to expect that T_{IS} represents the same type of characteristic temperatures, independent of systems. Because crystallization and glass transition temperatures are intrinsically different, it would be bizarre if T_{IS} agrees with the crystallization temperature for monodisperse systems but the glass transition temperature for bidisperse systems. Then, the question is whether T_{IS} indeed reflects any known temperature or it just happens to capture the density dependence of some characteristic temperatures qualitatively.

To answer this question, it is necessary to directly compare all these temperatures. For all thermal systems, we perform molecular dynamics simulations in the canonical ($NρT$) ensemble, collecting data after relaxing the system over a long time. We locate the characteristic temperatures from the liquid side by successively decreasing the temperature. For monodisperse systems, the crystallization temperature T_c is defined as the temperature at which the pressure p shows a discontinuous jump with the decrease of temperature. For bidisperse systems, we calculate the intermediate scattering function

$$F_s(k,t) = \frac{1}{N'} \left\langle \sum_j \exp\left(i\vec{k} \cdot [\vec{r}_j(t) - \vec{r}_j(0)] \right) \right\rangle \quad (6)$$

where $\langle . \rangle$ denotes the ensemble average and all the other symbols are the same as those in Eq. 1, from which the relaxation time τ satisfying $F_s(k, τ) = e^{-1} F_s(k,0)$ is obtained. Figure 2A shows some examples of $F_s(k, t)$ at various temperatures. The glass transition temperature T_g is determined by fitting the low-temperature part of $τ(T)$ in Fig. 2B into the Vogel-Fulcher function, $τ = τ_0 \exp[M/(T − T_g)]$, where $τ_0$ and M are fitting parameters.

In Fig. 2C, we first compare T_{IS} with T_g of bidisperse systems and T_c of monodisperse systems for all systems shown in Fig. 1. While T_c seems to quantitatively agree with T_{IS}, T_g is apparently lower than T_{IS}. The comparison indicates that T_{IS} may reflect the crystallization temperature but is not related to the glass transition temperature. The agreement between T_{IS} and T_c at least suggests that T_{IS} should not be a meaningless quantity, but the question is what T_{IS} represents for bidisperse systems.

Note that for glass-formers, there is another characteristic temperature named as the onset temperature, which separates the high-temperature simple liquids from the low-temperature "landscape-influenced" supercooled liquids (*23, 45*). As shown in Fig. 2B, the relaxation time $τ(T)$ at high temperatures is Arrhenius: $τ = τ_a \exp(E_a/T)$ with $τ_a$ and E_a being the prefactor and activation energy, respectively. This is a typical behavior of simple liquids. The Arrhenius behavior is destroyed and replaced with the super-Arrhenius behavior described
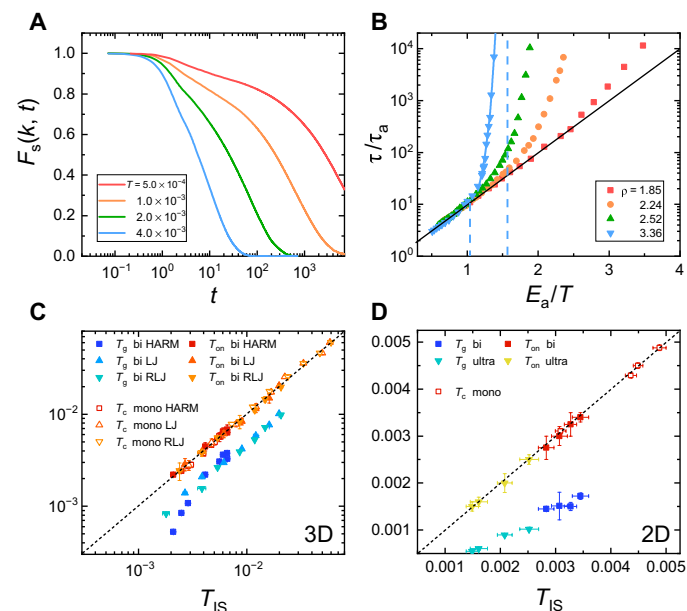
Fig. 2. Characteristic temperatures of thermal systems and their relations to T_{IS}. (**A**) Temperature evolution of the intermediate scattering function $F_s(k, t)$ for 3D HARM systems at ρ = 1.8. (**B**) Relaxation time $τ(T)$ for 3D HARM systems at various densities. The black and blue solid lines show the Arrhenius behavior at high temperatures and the Vogel-Fulcher fit at low temperatures, respectively. The vertical dashed lines mark the onset temperature T_{on} (left) and the glass transition temperature T_g (right), respectively. (**C** and **D**) Comparison between T_{IS} and characteristic temperatures such as T_g and T_{on} and the crystallization temperature T_c for 3D systems and 2D HARM systems, respectively. The dashed lines show where the characteristic temperatures are equal to T_{IS}. In (D), results of ultrastable inherent structures are shown for comparison.

by, for example, the Vogel-Fulcher function, when the temperature is lower than the onset temperature T_{on}. It is then interesting to know whether T_{IS} of bidisperse systems can agree with T_{on}.

We then compare T_{on} with T_{IS} in Fig. 2C. They turn out to agree well. Recent studies have proposed that T_{on} is consistent with the melting (crystallization) temperature (23, 45–47), especially a direct illustration of the quantitative agreement between them (47). The fact that both T_c and T_{on} agree with T_{IS} provides a strong piece of evidence linking the onset temperature of glass-formers to the crystallization temperature from the unique perspective of inherent structures. It is also intriguing that the calculation of T_{IS} from nonequilibrium inherent structures results in equilibrium temperatures.

Dependence on spatial dimension and quench rate

It is well known that due to the interference of interfacial energy, there is a hysteresis effect in the crystallization and melting processes for some materials so that the melting temperature T_m is higher than T_c. As shown in Fig. 3A, taking the 3D monodisperse HARM systems as the example, there is indeed a hysteresis effect. Here, we find that T_{IS} agrees with T_c but not T_m. A possible explanation is that T_c is the lower temperature limit for liquids with Arrhenius behavior to exist, while T_{on} plays the same role. In Fig. 3 (B and C), we show that liquids between T_m and T_c still exhibit an exponentially decayed $F_s(k, t)$ and an Arrhenius $\tau(T)$, similar to the behaviors of simple liquids above T_{on} for glass-formers.

In 2D, the hysteresis effect is weak and $T_m \approx T_c$, as shown in Fig. 3D. If T_{IS} could still agree with T_c, the link between T_{IS} and the crystallization (melting) process would be less vague. In Fig. 2D, we compare T_{IS} with T_c for 2D monodisperse HARM systems. They turn out to agree well. Figure 2D also shows that $T_{IS} \approx T_{on} > T_g$ for 2D bidisperse systems. Therefore, our argument that T_{IS} is connected to T_c and T_{on} does not rely on spatial dimension.

Another issue probably affecting the robustness of our argument is the quench rate. We calculate T_{IS} for ultrastable inherent structures obtained from the swap Monte Carlo algorithm. As shown in Fig. 2D, T_{IS} still matches well with T_{on} of the corresponding polydisperse system but is larger than T_g. Ultrastable inherent structures correspond to extremely slow quench rates. Therefore, our argument does not depend on quench rate, either.

Effective temperatures

Although derived from the FDR, T_{IS} is obtained in the absence of dynamics, different from previous studies of effective temperatures in typical nonequilibrium systems such as aging glasses, shear flows, and active matter (10–17, 48–50). It is then important to know the relationship between T_{IS} and previously defined effective temperatures. Can T_{IS} be the effective temperature of any or all these systems in the slow dynamics limit?

We then calculate the time-dependent FDR for bidisperse systems of aging glasses, quasi-static shear flows, and quasi-static self-propelled active flows. The time-dependent correlation and response functions are calculated as $C(t) = \langle \rho_k(t + t_w) \rho_k(t_w) \rangle_0 - \langle \rho_k(t_w) \rangle_0^2$ and $R(t) = [\langle \rho_k(t + t_w) \rangle_h - \langle \rho_k(t + t_w) \rangle_0]/h$, where t_w is the waiting time and $\langle . \rangle$ denotes the ensemble average with the subscript showing the strength of the perturbation field h.

Figure 4 (A and B) shows an example of $C(t)$ and $R(t)$, respectively, for an aging glass of HARM systems in 3D. To study the aging, we suddenly drop the temperature of the equilibrium liquid below the glass transition temperature and take the measurement after a
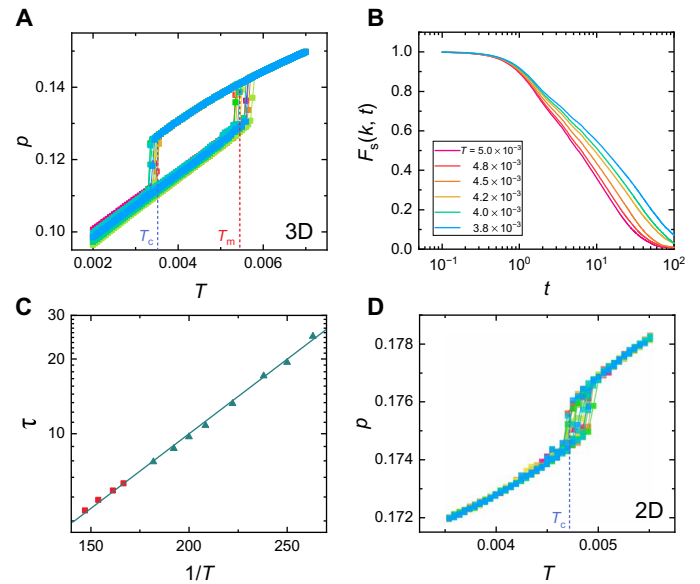
Fig. 3. Hysteresis effect in crystallization and melting. (**A**) Equation of state $p(T)$ for 3D monodisperse HARM systems at $\rho = 1.5$. We repeat the cooling and heating processes for multiple times (in different colors), and the hysteresis always exists. The vertical dashed lines label the crystallization temperature T_c and melting temperature T_m. (**B**) Intermediate scattering function $F_s(k, t)$ for states at $T_c < T < T_m$. They all show roughly exponential decay. (**C**) Temperature dependence of the relaxation time τ of liquid states above T_c. The squares and triangles are above and below T_m. The line is the Arrhenius fit to $\tau(T)$. Systems at $T_c < T < T_m$ still exhibit Arrhenius behavior. (**D**) Equation of state for 2D monodisperse HARM systems at $\rho = 1.4$. We also show multiple cooling-heating cycles. The vertical dashed line labels T_c. The hysteresis effect is weak in 2D systems.

waiting time t_w. With the increase of time, $C(t)$ decays, while $R(t)$ increases.

When we plot $R(t)$ against $C(t)$, as shown in Fig. 4C, there are apparently two distinct short- and long-time behaviors. This is different from equilibrium systems. It is well known that equilibrium systems show a linear $R(C)$ at all times and the temperature can be calculated from the slope of the $R(C)$ curve: $T = -\frac{dC(t)}{dR(t)}$. As discussed in most of previous studies (11–17, 48–50), the slope $\frac{dC(t)}{dR(t)}$ is time dependent for nonequilibrium systems. If we still define temperature from the slope, the temperature will vary with time. At short times, $-\frac{dC(t)}{dR(t)}$ is approximately equal to the heat bath temperature T. With the increase of time, $R(C)$ first exhibits a nonlinear crossover and then becomes linear at long times, from which the effective temperature $T_{eff} = -\frac{dC(t)}{dR(t)}$ is defined. It has been shown that the effective temperature is independent of waiting time t_w (48). In Fig. 4C, we compare $R(C)$ curves of aging glasses at three different temperatures. Although their heat bath temperatures are different, their $R(C)$ curves are parallel at long times, indicating that they have the same T_{eff}.

Remember that we intend to see whether there are any connections between T_{IS} and T_{eff}. Therefore, in Fig. 4D, we compare T_{eff} of aging glasses at various temperatures with T_{on}, which is T_{IS} for bidisperse systems. They all agree well with T_{on}.

Then, we repeat the work for quasi-static shear flows and quasi-static self-propelled active flows and show the results in Fig. 4 (E to H). The simulation details of both types of flows are described in Materials and Methods. For both types of flows, the waiting time t_w is sufficiently large to guarantee that the measurements are taken in steady flows.
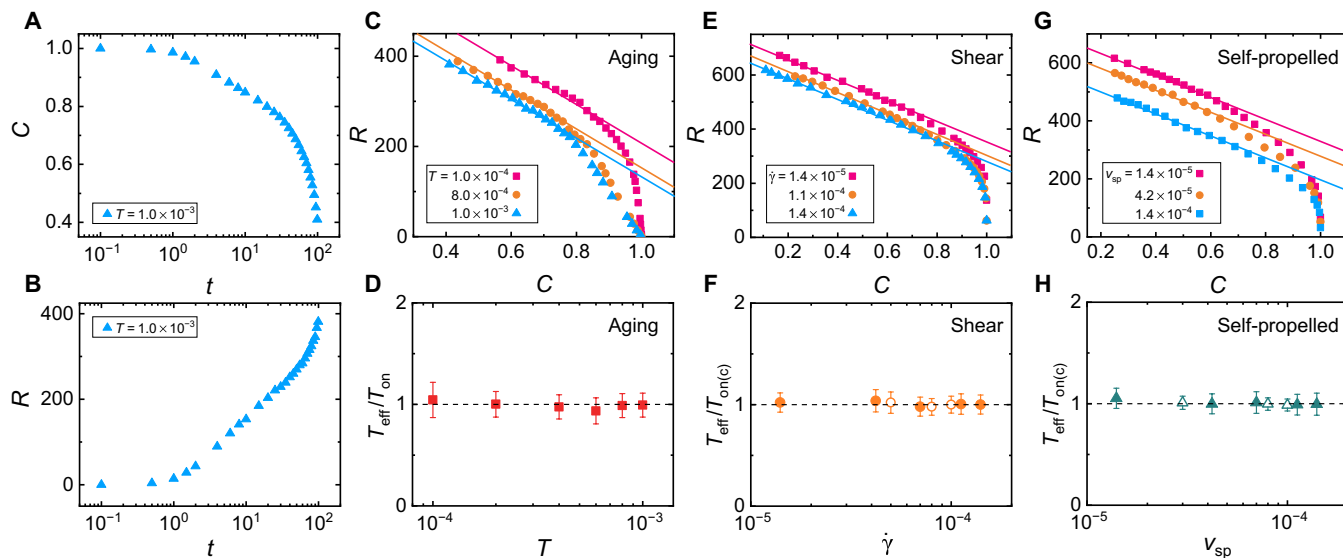
Fig. 4. Effective temperatures of slow-evolving HARM systems and their relations to the onset or crystallization temperatures. If not specified, the results are for 3D bidisperse systems at $\rho = 2.0$. (**A** and **B**) Correlation function $C(t)$ and response function $R(t)$ of an aging glass at $T = 10^{-3}$ and with $t_w = 10^4$. (**C**, **E**, and **G**) Relation between $R(t)$ and $C(t)$ for aging glasses at various temperatures T and with $t_w = 10^4$, quasi-static shear flows at various shear rates $\dot{\gamma}$, and quasi-static self-propelled flows at various self-propulsion velocities v_{sp}, respectively. The lines show the long-time linear FDR, from which the effective temperature T_{eff} is determined. (**D**, **F**, and **H**) Ratio of the effective temperature to the onset temperature, T_{eff}/T_{on}, against the temperature T for aging glasses, shear rate $\dot{\gamma}$ for shear flows, and self-propulsion velocity v_{sp} for self-propelled flows, respectively. The horizontal dashed lines show $T_{eff} = T_{on}$. In (F) and (H), we also show results of 3D monodisperse systems (empty symbols), and T_{eff} is compared with the crystallization temperature T_c.

Figure 4 (E and G) show that for both flows, $R(C)$ curves are also linear at long times and parallel for different shear rates $\dot{\gamma}$ or self-propulsion velocities v_{sp} studied here. As shown in Fig. 4 (F and H), in the quasi-static flow regime, T_{eff} is also equal to T_{on} for both sheared and self-propelled systems.

Now, we see that T_{eff} of aging glasses, quasi-static shear flows, and quasi-static self-propelled flows all agree with T_{on} (T_{IS}) for bidisperse systems. According to our argument that $T_{IS} \approx T_c$ for monodisperse systems, if T_{eff} of slow-evolving systems indeed reflects T_{IS}, we should see $T_{eff} \approx T_c$ for monodisperse systems. In Fig. 4 (F and H), we also compare T_{eff} of quasi-statically sheared and self-propelled monodisperse HARM systems. As expected, $T_{eff} \approx T_c$.

Figures 5 and 6 are counterparts of Fig. 4 for bidisperse LJ and RLJ systems in 3D. They tell the same story. On the basis of the results of Figs. 4 to 6, we are able to claim that T_{IS} measures the effective (fluctuation-dissipation) temperatures of slow-evolving nonequilibrium systems, independent of particle interactions and ways to drive the system to evolve. Therefore, our results suggest that fluctuation-dissipation temperatures of slow-evolving nonequilibrium systems may not be so mysterious as initially imagined. They all reflect the characteristic equilibrium temperatures, crystallization, and onset temperatures. This also provides another evidence of the connection between T_c and T_{on}.
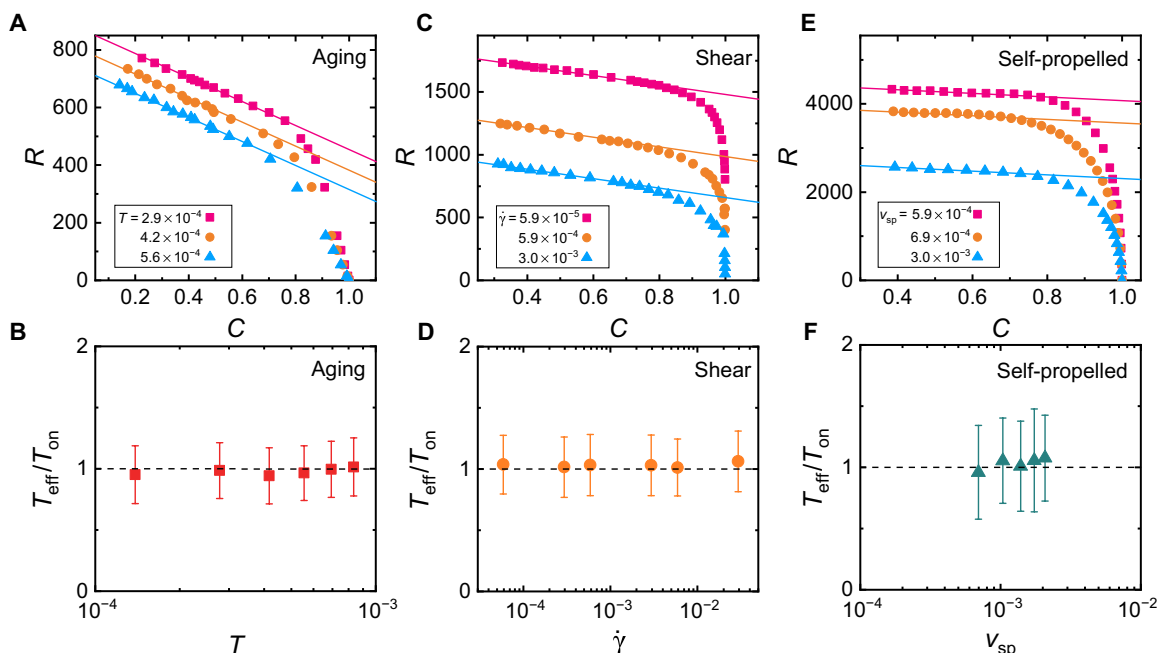
DISCUSSION

By calculating the FDR of inherent structures, we obtain a temperature-like quantity T_{IS}, which agrees well with the crystallization temperature of monodisperse systems and the onset temperature of bi- and polydisperse glass-formers. This statistical approach of inherent structures is crucial in several aspects. First, it shows that inherent

structures have the predictive power of characteristic temperatures of equilibrium systems, providing another evidence of the underlying connections between equilibrium and nonequilibrium systems (*41*). Second, it suggests a fast and easy way to indirectly calculate the crystallization and onset temperatures. Third, it evidences that the onset temperature and the crystallization temperature are essentially consistent.

Then, the question is why T_{IS} agrees with T_c and T_{on}. Note that T_{IS} is calculated from the FDR of inherent structures. It thus assumes the "exploration" of inherent structures even in the absence of dynamics. In this sense, T_{IS} could be regarded as the effective temperature at $T = 0$, which may correspond to the lowest heat bath temperature required to drive the system to traverse the potential energy landscape by overcoming energy barriers and explore all inherent structures. For monocomponent crystal-formers, the crystallization temperature T_c naturally acts as such a kind of temperature, because when $T < T_c$, the system crystallizes and loses the ability to freely explore the potential energy landscape. We do find that $T_{IS} \approx T_c$, consistent with our expectation. For glass-formers, previous studies have suggested that the onset temperature T_{on} plays a similar role as T_c (*23*, *45–47*). It is then reasonable to expect that T_{IS} agrees with T_{on} for glass-formers, which is exactly what we find here. Conversely, $T_{IS} \approx T_{on}$ and $T_{IS} \approx T_c$ found here directly illustrate the consistency between T_{on} and T_c. Of course, the situation is more complicated for glass-formers. Unlike crystals at $T < T_c$, supercooled liquids at $T < T_{on}$ can still diffuse. However, it is well known that systems at $T < T_{on}$ are in the landscape-influenced regime and selective of configurations (*23*), showing special dynamics distinct from simple liquids at $T > T_{on}$ such as two-step structural relaxation and dynamic heterogeneity (*39*, *51*, *52*). The fact that $T_{IS} \approx T_{on}$ consistently reflects that the system starts to explore the potential energy landscape in a way different from simple liquids when $T < T_{on}$.
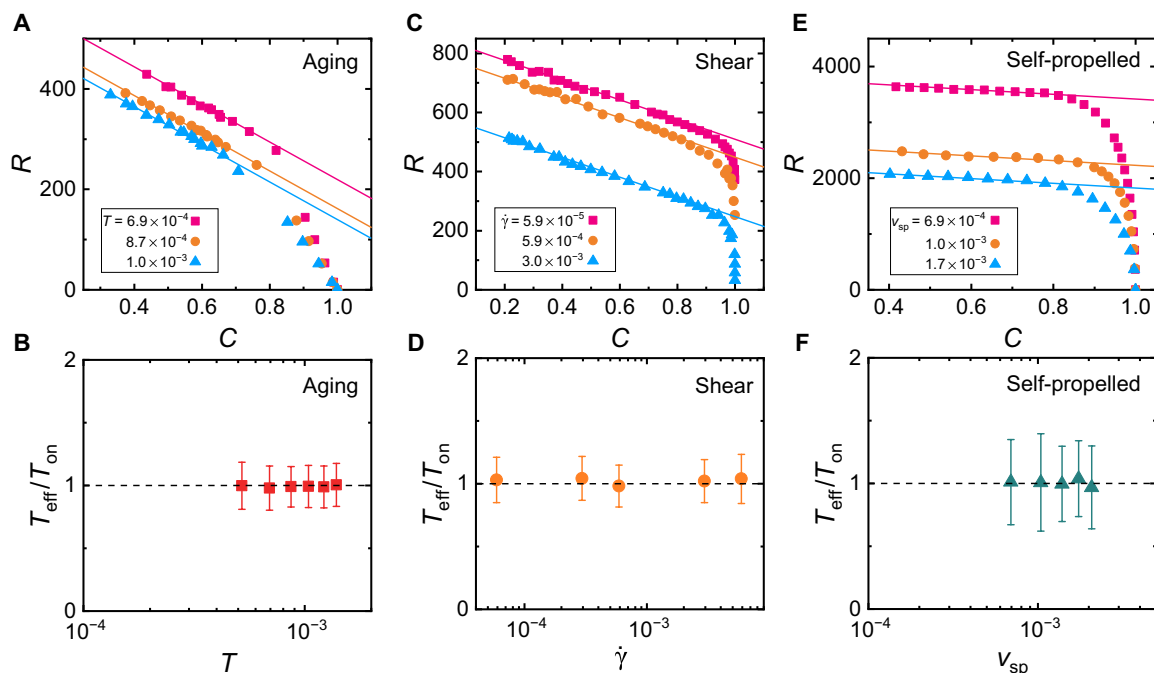
Fig. 5. Effective temperatures of slow-evolving bidisperse LJ systems and their relations to the onset temperatures. The results are for 3D systems at $\rho = 1.2$. (**A**, **C**, and **E**) Relation between $R(t)$ and $C(t)$ for aging glasses at various temperatures T and with $t_w = 10^3$, quasi-static shear flows at various shear rates $\dot{\gamma}$, and quasi-static self-propelled flows at various self-propulsion velocities v_{sp}, respectively. The lines show the long-time linear FDR, from which the effective temperature T_{eff} is determined. (**B**, **D**, and **F**) Ratio of the effective temperature to the onset temperature, T_{eff}/T_{on}, against the temperature T for aging glasses, shear rate $\dot{\gamma}$ for shear flows, and self-propulsion velocity v_{sp} for self-propelled flows, respectively. The horizontal dashed lines show $T_{eff} = T_{on}$.

Fig. 6. Effective temperatures of slow-evolving bidisperse RLJ systems and their relations to the onset temperatures. The results are for 3D systems at $\rho = 1.2$. (**A**, **C**, and **E**) Relation between $R(t)$ and $C(t)$ for aging glasses at various temperatures T and with $t_w = 10^3$, quasi-static shear flows at various shear rates $\dot{\gamma}$, and quasi-static self-propelled flows at various self-propulsion velocities v_{sp}, respectively. The lines show the long-time linear FDR, from which the effective temperature T_{eff} is determined. (**B**, **D**, and **F**) Ratio of the effective temperature to the onset temperature, T_{eff}/T_{on}, against the temperature T for aging glasses, shear rate $\dot{\gamma}$ for shear flows, and self-propulsion velocity v_{sp} for self-propelled flows, respectively. The horizontal dashed lines show $T_{eff} = T_{on}$.

Although easy to crystallize, monodisperse systems can still form glasses with sufficiently fast quench rates. We may then view T_c as T_{on} for the glass-formation of monodisperse systems on the basis of the consistency between T_c and T_{on}. On the other hand, widely used glass-formers, especially bidisperse systems, may slowly evolve to microphase or phase separation with sufficiently slow quench rate (41, 53). If phase separation occurs, T_{on} could be regarded as the onset temperature of the separation (ordering) as well. Therefore, whether crystals (phase separation) or glasses are formed is usually time dependent for some materials. However, T_{IS} has nothing to do with time, so does the characteristic temperature it represents, i.e., the lowest temperature for simple liquids with the Arrhenius behavior to exist. Below such a temperature, crystallization (phase separation) and glass-formation can occur at different time scales, but both processes exhibit dynamics deviating from the Arrhenius behavior. Then, how to interpret the temperature represented by T_{IS} (as T_c or T_{on}) depends on the form of the resultant solid.

Under certain conditions, bi-disperse systems can also form complex crystals such as Laves phases (54). In the parameter space studied in this work, we do not see any sign of the formation of complex crystals. If complex crystals could be formed, we expect that T_{IS} would still measure the crystallization temperature on the basis of our findings here. This requires the realization of complex crystals, which is beyond the scope of this work and will be left for future studies.

Acting as the zero-temperature effective temperature, T_{IS} unifies fluctuation-dissipation temperatures of typical slow-evolving non-equilibrium systems, such as aging glasses, shear flows, and self-propelled active matter. This clarifies the long-standing puzzles about the effective temperature: what the effective temperature defined from the FDR represents and whether it is a well-defined thermodynamic temperature unique to nonequilibrium systems. Our work reveals that it actually reflects the characteristic temperatures of equilibrium systems. For given systems, the crystallization or onset temperature is just a function of density. Therefore, once the density if fixed, the effective temperature of the corresponding slow-evolving system is fixed. In another word, the effective temperature is governed by density. If such an effective temperature could act as a thermodynamic temperature as the heat bath temperature in equilibrium systems does, it would obey the zeroth law of thermodynamics. Namely, for example, if we put two quasi-static shear flows with different effective temperatures into thermal contact, i.e., allowing heat to transfer between them, then we would expect that the effective temperature gradient causes "heat" flux to equilibrate the temperatures and, lastly, their effective temperatures are equal, although no particle exchange is allowed between the two systems and their densities are not allowed to change. However, this cannot happen (49). Because effective temperatures are controlled by density, as long as the densities of the two contacting shear flows are fixed, the effective temperature gap between them will maintain and no heat flux can be produced. Our work thus calls for the revisit of the effective temperature and the theories based on it. Being possibly the simplest case, the effective temperature of sheared ideal gases and its multiple definitions (6, 7) may be the good starting point.

MATERIALS AND METHODS
System details
Our systems are equilateral boxes with a side length L, containing $N = 1000$ (1024) particles with the same mass m in 3D (2D). In bidisperse

systems, there are N_A A particles and $N_B (= N - N_A)$ B particles, while $N_A = N$ and there are only A particles in monodisperse systems. We apply Lees-Edwards boundary conditions (55) when studying shear flows and periodic boundary conditions in all directions for all the other cases.

For LJ and RLJ systems, the interaction potential between particles i and j is

$$U(r_{ij}) = \frac{\epsilon_{ij}}{72}\left[\left(\frac{\sigma_{ij}}{r_{ij}}\right)^{12} - \left(\frac{\sigma_{ij}}{r_{ij}}\right)^6\right] + f(r_{ij}) \qquad (7)$$

where r_{ij} is the separation between the two particles, σ_{ij} and ϵ_{ij} depend on the types of interacting particles, and $f(r_{ij})$ ensures that $U = U' = 0$ at the truncation $r_{ij} = r_{ij}^c$. For bidisperse systems, we use the Kob-Anderson model (56): $N_A = 0.8 N$ and $N_B = 0.2 N$ with the parameters $\epsilon_{AB} = 1.5\epsilon_{AA}$, $\epsilon_{BB} = 0.5\epsilon_{AA}$, $\sigma_{AB} = 0.8\sigma_{AA}$, and $\sigma_{BB} = 0.88\sigma_{AA}$. The potential cutoff r_{ij}^c is $2.5\sigma_{ij}$ for LJ potential and $2^{1/6}\sigma_{ij}$ for RLJ potential.

For HARM systems, the interaction potential is

$$U(r_{ij}) = \frac{\epsilon}{2}\left(1 - \frac{r_{ij}}{\sigma_{ij}}\right)^2 \Theta\left(1 - \frac{r_{ij}}{\sigma_{ij}}\right) \qquad (8)$$

where σ_{ij} is the sum of radii of particles i and j, and $\Theta(x)$ is the Heaviside step function. For bidisperse systems, $N_A = N_B = 0.5 N$ and the diameters of A and B particles are σ_0 and $\sigma_0/1.4$, respectively. We also use polydisperse HARM systems to efficiently generate ultrastable inherent structures. For polydisperse systems, the particle diameters σ are chosen from the distribution $P(\sigma) \sim \sigma^{-3}$, where $\sigma \in [0.73\sigma_0, 1.63\sigma_0]$.

Calculation of onset temperature
To locate the onset temperature, we fit the intermediate scattering function $F_s(k, t)$ with the Kohlrausch-Williams-Watts stretched exponential form, $F_s(k, t) \sim \exp[(t/\tau)^\beta]$. For simple liquids with Arrhenius behavior, $\beta = 1$. When $T < T_{on}$ and the liquids exhibit super-Arrhenius behavior, $\beta < 1$. We set T_{on} as the temperature at which β decays to $0.8 \sim 0.9$ (57, 58).

Simulation of shear flows
To mimic shear flows, we apply the shear in the x direction with a shear rate $\dot{\gamma}$ and integrate the equation of motion

$$m\frac{d^2\vec{r}_i}{dt^2} = -\sum_j\left[\frac{dU(r_{ij})}{d\vec{r}_i} + \eta(\vec{v}_i - \vec{v}_j)\right] \qquad (9)$$

where $\vec{r}_i$ and $\vec{v}_i$ are the location and velocity of particle i, η is the damping coefficient, and the sum is over all particles interacting with particle i. Here, we use $\eta = 0.5$ in units to be defined below.

Simulation of self-propelled flows
For self-propelled active systems, we study a minimal model governed by the overdamped equation of motion (59)

$$\chi\vec{v}_i = -\sum_j\frac{dU(r_{ij})}{d\vec{r}_i} + f\vec{n}_i = \vec{F}_i + f\vec{n}_i \qquad (10)$$

where χ is the damping coefficient, f and $\vec{n}_i$ are the strength and orientation of self-propulsion, respectively, and the sum is over all

particles interacting with particle i. The orientation $\vec{n}_i$ is set at the beginning of the simulation and remains fixed, satisfying $\sum_i \vec{n}_i = 0$. To probe quasi-static flows of self-propelled particles [see (60) for the reasons in detail], we use a recently developed constant propulsion velocity algorithm (60) by setting

$$ f = \chi v_{\text{sp}} - \frac{1}{N} \sum_{i=1}^{N} \vec{F}_i \cdot \vec{n}_i \qquad (11) $$

where $v_{\text{sp}} = \frac{1}{N} \sum_{i=1}^{N} \vec{v}_i \cdot \vec{n}_i$ is the average self-propulsion velocity. Then, we are able to control v_{sp} and access quasi-static flows in the $v_{\text{sp}} \to 0$ limit.

Units

For LJ and RLJ systems, we set the units of length, mass, and energy to be σ_{AA}, m, and ϵ_{AA}, respectively. The temperature is in units of $\epsilon_{AA} k_B^{-1}$ with k_B being the Boltzmann constant. The density ρ is defined as $N \sigma_{AA}^3 L^{-3}$. For self-propelled systems with $m = 0$, the time is in units of $\chi \sigma_{AA}^2 / \epsilon_{AA}$. For all the other systems, the time is in units of $m^{1/2} \sigma_{AA} \epsilon_{AA}^{-1/2}$. For HARM systems, we replace σ_{AA} and ϵ_{AA} with σ_0 and ϵ.

REFERENCES AND NOTES

1. National Research Council, *Condensed-Matter and Materials Physics: The Science of the World Around Us* (The National Academies Press, 2007).
2. H. Jaeger, A. J. Liu, *Far-From-Equilibrium Physics: An Overview* (2010); arXiv:1009.4874.
3. J. G. Powles, G. Rickayzen, D. M. Heyes, Temperatures: Old, new, and middle aged. *Mol. Phys.* **103**, 1361–1373 (2005).
4. A. Puglisi, A. Sarracino, A. Vulpiani, Temperature in and out of equilibrium: A review of concepts, tools, and attempts. *Phys. Rep.* **709-710**, 1–60 (2017).
5. J. Casas-Vázquez, D. Jou, Temperature in non-equilibrium states: A review of open problems and current proposals. *Rep. Prog. Phys.* **66**, 1937–2023 (2003).
6. M. Criado-Sancho, D. Jou, J. Casas-Vázquez, Nonequilibrium kinetic temperatures in flowing gases. *Phys. Lett. A* **350**, 339–341 (2006).
7. D. Jou, M. Criado-Sanchoc, J. Casas-Vázquez, Nonequilibrium temperature and fluctuation-dissipation temperature in flowing gases. *Physica A* **358**, 49–57 (2005).
8. J. Kurchan, Emergence of macroscopic temperatures in systems that are not thermodynamical microscopically: Towards a thermodynamical description of slow granular rheology. *J. Phys. Condens. Matter* **12**, 6611 (2000).
9. A. Crisanti, F. Ritort, Violation of the fluctuation-dissipation theorem in glassy systems: Basic notions and the numerical evidence. *J. Phys. A Math. Gen.* **36**, R181–R290 (2003).
10. H. A. Makse, J. Kurchan, Testing the thermodynamic approach to granular matter with a numerical model of a decisive experiment. *Nature* **415**, 614–617 (2002).
11. L. F. Cugliandolo, J. Kurchan, L. Peliti, Energy flow, partial equilibration, and effective temperatures in systems with slow dynamics. *Phys. Rev. E* **55**, 3898–3914 (1997).
12. L. Berthier, J. L. Barrat, Nonequilibrium dynamics and fluctuation-dissipation relation in a sheared fluid. *J. Chem. Phys.* **116**, 6228–6242 (2002).
13. L. Berthier, J. L. Barrat, Shearing a glassy material: Numerical tests of nonequilibrium mode-coupling approaches and experimental proposals. *Phys. Rev. Lett.* **89**, 095702 (2002).
14. S. Fielding, P. Sollich, Observable dependence of fluctuation-dissipation relations and effective temperatures. *Phys. Rev. Lett.* **88**, 050603 (2002).
15. Q. Chen, M.-Y. Hou, Effective temperature and fluctuation-dissipation theorem in athermal granular systems: A review. *Chinese Phys. B* **23**, 074501 (2014).
16. C. S. O'Hern, A. J. Liu, S. R. Nagel, Effective temperatures in driven systems: Static versus time-dependent relations. *Phys. Rev. Lett.* **93**, 165702 (2004).
17. R. Di Leonardo, L. Angelani, G. Parisi, G. Ruocco, Off-equilibrium effective temperature in monatomic Lennard-Jones glass. *Phys. Rev. Lett.* **84**, 6054–6057 (2000).
18. U. Seifert, T. Speck, Fluctuation-dissipation theorem in nonequilibrium steady states. *Europhys. Lett.* **89**, 10007 (2010).
19. G. Verley, K. Mallick, D. Lacoste, Modified fluctuation-dissipation theorem for nonequilibrium steady states and applications to molecular motors. *Europhys. Lett.* **93**, 10002 (2011).
20. F. H. Stillinger, T. A. Weber, Computer-simulation of local order in condensed phases of silicon. *Phys. Rev. B* **31**, 5262–5271 (1985).
21. P. G. Debenedetti, F. H. Stillinger, Supercooled liquids and the glass transition. *Nature* **410**, 259–267 (2001).
22. H. C. Andersen, Molecular dynamics studies of heterogeneous dynamics and dynamic crossover in supercooled atomic liquids. *Proc. Natl. Acad. Sci.* **102**, 6686–6691 (2005).
23. S. Sastry, P. G. Debenedetti, F. H. Stillinger, Signatures of distinct dynamical regimes in the energy landscape of a glass-forming liquid. *Nature* **393**, 554–557 (1998).
24. A. Widmer-Cooper, H. Perry, P. Harrowell, D. R. Reichman, Irreversible reorganization in a supercooled liquid originates from localized soft modes. *Nat. Phys.* **4**, 711–715 (2008).
25. L. Wang, Y. Duan, N. Xu, Non-monotonic pressure dependence of the dynamics of soft glass-formers at high compressions. *Soft Matter* **8**, 11831–11838 (2012).
26. M. L. Manning, A. L. Liu, Vibrational modes identify soft spots in a sheared disordered packing. *Phys. Rev. Lett.* **107**, 108302 (2011).
27. K. Chen, M. L. Manning, P. J. Yunker, W. G. Ellenbroek, Z. X. Zhang, A. J. Liu, A. G. Yodh, Measurement of correlations between low-frequency vibrational modes and particle rearrangements in quasi-two-dimensional colloidal glasses. *Phys. Rev. Lett.* **107**, 108301 (2011).
28. N. Xu, A. J. Liu, S. R. Nagel, Instabilities of jammed packings of frictionless spheres under load. *Phys. Rev. Lett.* **119**, 215502 (2017).
29. H. Tong, N. Xu, Order parameter for structural heterogeneity in disordered solids. *Phys. Rev. E* **90**, 010401(R) (2014).
30. L. Wang, N. Xu, Probing the glass transition from structural and vibrational properties of zero-temperature glasses. *Phys. Rev. Lett.* **112**, 055701 (2014).
31. L. Berthier, D. Coslovich, A. Ninarello, M. Ozawa, Equilibrium sampling of hard spheres up to the jamming density and beyond. *Phys. Rev. Lett.* **116**, 238002 (2016).
32. D. Chandler, *Introduction to Modern Statistical Mechanics* (Oxford Univ. Press, 1987).
33. E. Bitzek, P. Koskinen, F. Gähler, M. Moseler, P. Gumbsch, Structural relaxation made simple. *Phys. Rev. Lett.* **97**, 170201 (2006).
34. J. D. Weeks, D. Chandler, H. C. Andersen, Role of repulsive forces in determining the equilibrium structure of simple liquids. *J. Chem. Phys.* **54**, 5237–5247 (1971).
35. L. Berthier, G. Tarjus, The role of attractive forces in viscous liquids. *J. Chem. Phys.* **134**, 214503 (2011).
36. L. Berthier, G. Tarjus, Nonperturbative effect of attractive forces in viscous liquids. *Phys. Rev. Lett.* **103**, 170601 (2009).
37. N. Gnan, C. Maggi, T. B. Schrøder, J. C. Dyre, Predicting the effective temperature of a glass. *Phys. Rev. Lett.* **104**, 125902 (2010).
38. U. R. Pedersen, T. B. Schrøder, J. C. Dyre, Repulsive reference potential reproducing the dynamics of a liquid with attractions. *Phys. Rev. Lett.* **105**, 157801 (2010).
39. L. Berthier, G. Biroli, Theoretical perspective on the glass transition and amorphous materials. *Rev. Mod. Phys.* **83**, 587–645 (2011).
40. S. A. Khrapak, G. E. Morfill, Accurate freezing and melting equations for the Lennard-Jones system. *J. Chem. Phys.* **134**, 094108 (2011).
41. Y. Nie, J. Liu, J. Guo, N. Xu, Connecting glass-forming ability of binary mixtures of soft particles to equilibrium melting temperatures. *Nat. Commun.* **11**, 3198 (2020).
42. C. N. Likos, Effective interactions in soft condensed matter physics. *Phys. Rep.* **348**, 267–439 (2001).
43. M. Zu, J. Liu, H. Tong, N. Xu, Density affects the nature of the hexatic-liquid transition in two-dimensional melting of soft-core systems. *Phys. Rev. Lett.* **117**, 085702 (2016).
44. C. S. O'Hern, L. E. Silbert, A. J. Liu, S. R. Nagel, Jamming at zero temperature and zero applied stress: The epitome of disorder. *Phys. Rev. E* **68**, 011306 (2003).
45. Y. Brumer, D. R. Reichman, Mean-field theory, mode-coupling theory, and the onset temperature in supercooled liquids. *Phys. Rev. E* **69**, 041202 (2004).
46. T. Yanagishima, J. Russo, H. Tanaka, Common mechanism of thermodynamic and mechanical origin for ageing and crystallization of glasses. *Nat. Commun.* **8**, 15954 (2017).
47. U. R. Pedersen, T. B. Schróder, J. C. Dyre, Phase diagram of Kob-Andersen-type binary Lennard-Jones mixtures. *Phys. Rev. Lett.* **120**, 165501 (2018).
48. L. Berthier, Efficient measurement of linear susceptibilities in molecular simulations: Application to aging supercooled liquids. *Phys. Rev. Lett.* **98**, 220601 (2007).
49. N. Xu, C. S. O'Hern, Effective temperature in athermal systems sheared at fixed normal load. *Phys. Rev. Lett.* **94**, 055701 (2005).
50. D. Loi, S. Mossa, L. F. Cuglindolo, Effective temperature of active matter. *Phys. Rev. E* **77**, 051111 (2008).
51. H. Tanaka, T. Kawasaki, H. Shintani, K. Watanabe, Critical-like behaviour of glass-forming liquids. *Nat. Mater.* **9**, 324–331 (2010).
52. E. R. Weeks, J. C. Crocker, A. C. Levitt, A. Schofield, D. A. Weitz, Three-dimensional direct imaging of structural relaxation near the colloidal glass transition. *Science* **287**, 627–631 (2000).
53. J. Russo, F. Romano, H. Tanaka, Glass forming ability in systems with competing orderings. *Phys. Rev. X* **8**, 021040 (2018).
54. A.-P. Hynninen, J. H. J. Thijssen, E. C. M. Vermolen, M. Dijkstra, A. van Blaaderen, Self-assembly route for photonic crystals with a bandgap in the visible region. *Nat. Mater.* **6**, 202–205 (2007).
55. M. P. Allen, D. J. Tildesley, *Computer Simulation of Liquids* (Oxford Univ. Press, 2017).

56. W. Kob, H. C. Andersen, Scaling behavior in the β-relaxation regime of a supercooled Lennard-Jones mixture. *Phys. Rev. Lett.* **73**, 1376–1379 (1994).

57. W. Kob, H. C. Andersen, Testing mode-coupling theory for a supercooled binary Lennard-Jones mixture. II. Intermediate scattering function and dynamic susceptibility. *Phys. Rev. E* **52**, 4134–4153 (1995).

58. A. Banerjee, M. K. Nandi, S. Sastry, S. M. Bhattacharyya, Determination of onset temperature from the entropy for fragile to strong liquids. *J. Chem. Phys.* **147**, 024504 (2017).

59. Y. Fily, M. C. Marchetti, Athermal phase separation of self-propelled particles with no alignment. *Phys. Rev. Lett.* **108**, 235702 (2012).

60. R. Mo, Q. Liao, N. Xu, Rheological similarities between dense self-propelled and sheared particulate systems. *Soft Matter* **16**, 3642–3648 (2020).

Citation: J. Zhang, W. Zheng, S. Zhang, D. Xu, Y. Nie, Z. Jiang, N. Xu, Unifying fluctuation-dissipation temperatures of slow-evolving nonequilibrium systems from the perspective of inherent structures. *Sci. Adv.* **7**, eabg6766 (2021).